Upgrading of flax powder and short fibers into high value-added products

Daniel Torres, Victor Medina Bailon, Judith Dominguez Mendoza, Eric Masson, Guillermo Gonzalez-Sanchez, Lourdes Ballinas-Casarrubias, Salima Mabrouk, Raphaël Schneider, Alain Celzard, Vanessa Fierro

Version of Record: https://www.sciencedirect.com/science/article/pii/S2213343722000689
Manuscript_9e351369adec5b4a09981583a6f85a29

Upgrading of flax powder and short fibers into high value-added products

Daniel Torres[1,2], Victor Medina Bailon[3], Judith Dominguez Mendoza[3], Eric Masson[4], Guillermo Gonzalez-Sanchez[3], Lourdes Ballinas-Casarrubias[5], Salima Mabrouk[1], Raphaël Schneider[1], Alain Celzard[2]*, Vanessa Fierro[2]*

[1] Université de Lorraine, CNRS, LRGP, F-54000 Nancy, France

[2] Université de Lorraine, CNRS, IJL, F-88000 Epinal, France

[3] Centro de Investigación en Materiales Avanzados (CIMAV), Chihuahua 31136, Mexico

[4] Critt bois, 27 rue Philippe Seguin, BP 91067, 88051 Épinal Cedex 9, France

[5] Facultad de Ciencias Químicas, Universidad Autónoma de Chihuahua, Circuito Universitario s/n, 31125 Chihuahua, Chih., Mexico

* Corresponding authors: E-mail address : Vanessa.Fierro@univ-lorraine.fr (Vanessa Fierro), Alain.Celzard@univ-lorraine.fr (Alain Celzard)

ABSTRACT

Lignocellulosic materials have great potential to be valorized into new products. Flax by-products such as powder and short fibers are used in the present study to identify plausible potential applications for the products obtained from their hydrothermal treatment. The as-received industrial flax by-products are subjected to hydrothermal carbonization (HTC) in a wide range of severity, an operating parameter combining time and temperature. In this way, the yield and characteristics of the resulting HTC products: hydrochars, carbon quantum dots (CQDs) and organics such as 5-hydroxymethylfurfural (5-HMF) and furfural (FU), are determined. Likewise, pyrolysis of the hydrochars and the starting flax by-products at 900 °C is also carried out, leading to carbon materials with developed surface areas, higher than 950 m^2/g, and CO_2 capture values of up to 4.8 mmol/g at 1 bar and 0 °C. In the overall process, severities above 4.9 were found to be optimal in terms of higher calorific value (around 27 MJ/kg) of the obtained hydrochars, production of organic products (0.22 and 0.06 g/L of 5-HMF and FU, respectively), photoluminescence quantum yield of the CQDs fraction (4.7%) and CO_2 capture (up to 4.8 mmol/g) by the hydrochar-derived carbons.

Keywords: hydrothermal carbonization; flax by-product valorization; hydrochar; carbon quantum dots; furfural

1 INTRODUCTION

Flax fiber has been used since ancient times, with evidence of use dating back 10,000 years (Yan et al., 2014). Europe supplies 80% of the world's production, mainly grown in France, Belgium and the Netherlands, with 140,000 tons of drained linen for a total of 160,000 hectares cultivated in 2020. In recent years, the use of flax fiber to replace glass fiber in composite materials has gained interest (Baley et al., 2016). Flax is also finding use in the paper and food industries. The largest flax fibers are used to manufacture high-value products, while the shortest ones and powder are often considered by-products that are difficult to upgrade (Akin, 2013).

Hydrothermal treatments, lately called hydrothermal carbonization (HTC), are processes that take place at moderate pressure and temperature and that have been used for processing lignocellulosic materials and valorizing the resultant liquid and solid fractions. This kind of process allows relatively insoluble materials to be dissolved under ordinary conditions to produce value-added chemicals. HTC is considered a green alternative for the treatment of biomass (Yoshimura and Byrappa, 2008). Pretreatment of lignocellulosic feedstocks concerns the ultrastructural modification of materials such as wood, straw and bagasse and they can be classified as follows: (i) steam; (ii) aqueous; and (iii) organosolvolysis treatments. All these treatments have their antecedents in the thermomechanical processes developed by the pulp and paper or fiberboard industries (Overend et al., 1987). Their application leads to a fractionation of the substrate into its main polymeric fractions: cellulose, hemicellulose and lignin with various degrees of modification. A number of pretreatment concepts now exist on a commercial scale, and they are applied to produce foodstuffs for ruminants from lignocellulosic raw materials. The same techniques are being experimented in the energy and chemical sectors from the same feedstocks, as these treatments are chemicals-free and drying of the biomass is not required (Yoshimura and Byrappa, 2008).

After subjecting biomass to HTC, the resultant liquid fraction contains small molecules such as formic or acetic acids, but also compounds with molecular weights above several thousand Da. Among the lighter molecules, furfural (FU) and 5-hydroxymethylfurfural (5-HMF) are among the most interesting. FU is produced industrially by acid hydrolysis of pentosans or directly from biomass (Harry et al., 2014; Steinbach et al., 2017; Yemiş and Mazza, 2011), while 5-HMF (not obtained on a large scale) is obtained from glucose and fructose (Catrinck et al., 2017; Dou et al., 2018; Lv et al., 2017). Additionally, low molecular weight carbon fractions remain dispersed in the liquid phase after HTC of biomass and may exhibit photoluminescence (PL) properties due to quantum confinement effects (Abbas et al., 2018; Thongsai et al., 2019; Zhao et al., 2020). These carbon quantum dots (CQDs) of renewable origin are biocompatible and have been used in applications such as bioimaging, biosensing, or optoelectronics and energy devices (Abbas et al., 2018; Das et al., 2018). On the other hand, solid products from HTC processes are becoming increasingly important as potential precursors of carbon-rich materials (Braghiroli et al., 2015a, 2015b, 2015b, 2014, 2012; Román et al., 2013; Wei et al., 2011). After carbonization of hydrochars, the resultant carbon materials may indeed have applications in catalysis, electrochemistry, energy storage, selective gas sequestration, water purification or soil amendment (Braghiroli et al., 2015c; Kang et al., 2012; Li et al., 2014; Schaefer et al., 2016; Steinbeiss et al., 2009; Titirici et al., 2012).

Although temperature and residence time are the most important parameters in the transformation of biomass, other parameters, such as the type of feedstock or use of catalysts can also affect the products obtained by HTC (Funke and Ziegler, 2010; Borrero-López et al., 2018). The objective of the present study was to explore the possible valorization of short fibers and flax powder by HTC under mild severity conditions and avoiding the use of catalysts. The effect of temperature and time on the hydrochar yield and its characteristics, as well as on the hydrochar-derived carbons, were therefore studied. Likewise, extracts from the process

including valuable liquids and dispersed CQDs were separated and duly analyzed. The results of this work show new application perspectives for low-value by-products from the linen industry.

2 EXPERIMENTAL

2.1 Raw materials

This work was carried out with two types of flax-derived products: short fiber fragments and powder, both provided by Depestele Group (France). The amount of lignin and cellulose were directly determined according to TAPPI standards T222 and T203, respectively, while hemicellulose was determined by difference. Moisture and ash contents were determined by application of ASTM E871 and E1755 standards, respectively.

Carbon, hydrogen, oxygen, nitrogen and sulfur contents were directly determined using a CHONS elemental analyzer (Vario EL Cube, Elementar, Germany).

Secondary electrons were used to observe the topographic contrast of the samples using a scanning electron microscope (FET Quanta 600 FEG) under an accelerating voltage of 3 kV. The EDX instrument of the microscope was used for microanalysis and mapping of the major elements.

2.2 Carbonization treatments

2.2.1 Hydrothermal carbonization (HTC)

Temperature and time are the most important variables in hot pressurized water treatments. The reaction coordinate, R_0, based on the combination of temperature, T (°C), and residence time, t (min), was defined by (Overend et al., 1987) to describe the impact of hot liquid water treatments on lignocellulosic components:

$$R_0 = t \cdot exp\left(\frac{T-100}{14.75}\right) \quad (1)$$

In Eq. (1), 14.75 is the activation energy (kJ/mol) based on the assumptions that the reaction is hydrolytic and that the overall conversion is first-order. The logarithm of the reaction coordinate, log R_0, was defined as the severity of hydrothermal carbonization, *i.e.*, what is known as the severity factor.

At a given temperature, the pressure inside the reactor was auto-generated by the pressurized water itself in the available volume of the autoclave. After the reaction time, the autoclave was removed from the oven and cooled to room temperature for several hours. The solids recovered after HTC, *i.e.*, the hydrochars, were separated from the remaining liquid phase by filtration, and were then washed with distilled water and dried in an oven at 80 °C for 8 hours. The hydrochar yield was defined as the ratio of the weight of hydrochar to that of the initial flax material on a dry basis.

The experimental details and conditions, which were studied in our own previous works (Borrero-López et al., 2018, 2020), are as follows. The HTC processes were performed in 125 mL Anton Parr autoclaves. Distilled water was used as the reaction medium, and the liquid to solid (L/S) weight ratio used was 45/2; i.e., 45 g of water and 2 g of flax powder or fiber. Flax material and water were introduced together in the autoclave reaction vessel, which in turn was installed in a ventilated oven preheated to the desired temperature. The temperature was varied from 130 to 180 °C, and different times were tested: 1, 2, 4, 6, 12 and 24 hours. The autoclave was then removed from the oven and left for several hours at room temperature to cool. The solid and liquid fraction were separated by filtration and weighed for subsequent analysis.

2.2.2 Hydrochar carbonization

The hydrochars obtained from the aforementioned HTC process were also further carbonized. For that purpose, approximately 1 g of hydrochar was placed in a previously weighed ceramic boat and introduced into a tubular furnace. The latter was continuously flushed by nitrogen flowing at 90 mL/min, and heated at 2 °C/min to 900 °C. This final temperature

was maintained for 1 hour before cooling to room temperature under N_2 flow. This procedure prevented any oxidation of the sample. The latter was then stored in a desiccator and weighed. The carbonization yield (Y_C) was calculated as the mass ratio of carbon material to hydrochar on a dry basis. The total carbon yield (Y_T) was also calculated as the mass ratio of the final carbon material to the raw flax powder or fiber, again on a dry basis.

2.3 Characterization of products

2.3.1 Liquid fractions

The analyses were carried out after liquid-liquid extraction using 3 mL of dichloromethane and 3 mL of the liquid fraction sample under vigorous stirring. Afterwards, the dichloromethane phase was removed from the solution and analyzed by GC/MS.

The first step of the liquid fraction analysis was performed by using a chromatograph coupled to a mass spectrometer (GC/MS) Clarus 500 (Perking Elmer Inc., USA) to identify the main compounds present in the samples. The analysis was carried out with a fused-silica capillary column (Rxi-5Sil MS; 30 m × 0.25 mm, 0.25 μm film thickness; Restek, USA). The gas chromatograph was equipped with an electronically controlled split/splitless injection port. The injection volume was 0.5 μL at 275 °C in splitless mode with a 1 min splitless time. Helium (Alphagaz 2, Air Liquide) was used as carrier gas, with a constant flow rate of 1 mL/min. The oven temperature program used was as follows: 40 °C fixed for 2 min, 40 °C to 325 °C at a rate of 7.5 °C/min, and then 325 °C fixed for 5 min. Ionization was performed in electron impact mode (ionization energy of 70 eV). The ion source and transfer line temperatures were 250 °C and 330 °C, respectively. Detection was carried out in scan mode, from m/z = 20 to 500. The detector was switched off in the initial 5.5 min (solvent delay). The compounds were identified by comparison with spectra from the NIST (US National Institute of Standards and Technology, USA) mass spectral library.

2.3.2 Hydrochars and porous carbons

The elemental analysis of the solid products was carried out in the same way as for the raw materials. In order to evaluate the realistic possibility of using hydrochars as a source of energy by combustion, their ash contents were determined by thermogravimetric analysis (TGA). This analysis was performed by increasing the temperature at 5 °C/min to 900 °C in a continuous flow of synthetic air. This final temperature was maintained for 1 hour.

The textural properties of the samples were determined from nitrogen adsorption-desorption isotherms at -196 °C and CO_2 adsorption at 0 °C, using Micromeritics ASAP 2020 and Micromeritics ASAP 2420 automatic adsorption devices, respectively. The BET (Brunauer-Emmet-Teller) method was used to determine the BET area, A_{BET} (m^2/g) (Brunauer et al., 1938). Particular attention was paid to the parameter C in the BET equation, which provides information about the interaction between the adsorbent surface and the adsorbate, and which must be positive. A_{BET} strongly depends on the range of relative pressures (P/P_0) chosen to fit the BET equation to the nitrogen isotherm, and thus cannot be applied automatically between 0.05 and 0.25. $V_{N2} \times (1\text{-}P/P_0)$ was thus plotted, where V_{N2} is the adsorbed nitrogen volume at a given value of P/P_0, as a function of P/P_0 and starting at $P/P_0 = 0.01$. The maximum P/P_0 to fit the BET equation is where $V_{N2} \times (1\text{-}P/P_0)$ reaches its maximum. The micropore volume, $V_{DR.N2}$ (cm^3/g), was determined using the Dubinin-Raduskevich method (Dubinin, 1989). The total pore volume accessible by adsorption, $V_{0.97}$ (cm^3/g), was measured at a relative nitrogen pressure of 0.97. The mesopore volume, V_{mes} (cm^3/g), was assumed to be the difference $V_{0.97} - V_{DR.N2}$. All data were treated using the MicroActive® software from Micromeritics. Finally, the pore size distribution (PSD) was determined by applying the non-local density functional theory (NLDFT), combining both N_2 and CO_2 adsorption isotherms using the SAIEUS® software provided by Micromeritics (Jagiello et al., 2015). The PSD was then used to calculate the

surface area, S_{NLDFT}, and the micropore volume, $V_{mic\ NLDFT}$. The average pore diameter, $d_{p,av}$, was calculated as:

$$\boldsymbol{d_{p,av}(nm) = 4 \cdot \frac{V_{0.97}}{S_{NLDFT}} \cdot 10^{-6}} \quad (2)$$

The tapped density is an upper bound of bulk density, reached after mechanically tapping a graduated measuring cylinder or vessel containing the powder sample. After measuring the mass and observing the initial volume of the powder, the measuring cylinder or vessel is mechanically tapped, and volume readings are taken until little change is observed. The tapped density was measured with an Autotap Equipment (Quantachrome). As it indicates the maximum density that can be achieved by a powdered solid, without compaction, it is useful in calculating volumes from the weight of the merchandise being transported.

The higher heating values (HHVs) of flax powders, fibers and hydrochars were determined by a calorimeter (Parr6400, Parr instrument, USA) according to the standard method for calorimetric analysis (EPA 5050). In this context, the term "higher" refers to the fact that the water produced by the combustion was condensed in the calorimeter (closed system), and therefore the heat of vaporization of water was not lost, leading to a higher calorific value than would be found in an open system.

2.3.3 Carbon quantum dots

Optical properties of CQDs were measured at room temperature and under ambient conditions. Absorption spectra were measured using a Thermo Scientific Evolution 220 UV-visible spectrophotometer (Thermo Fisher, France). Photoluminescence (PL) spectra were recorded with a Fluoromax-4 Jobin Yvon spectrofluorimeter (HORIBA Jobin Yvon, France). The PL spectra were spectrally corrected and PL quantum yields (PL QYs) were determined using quinine sulfate as reference ($QY(ref) = 0.54$) according to the equation:

$$QY(sample) = \left(\frac{F_{sample}}{F_{ref}}\right)\left(\frac{A_{ref}}{A_{sample}}\right)\left(\frac{n_{sample}^{\ 2}}{n_{ref}^{\ 2}}\right)QY_{(ref)} \quad (3)$$

where F is the integrated PL emission intensity (after excitation at 350 or 375 nm for CQDs derived from flax powder or short fibers, respectively, and for quinine sulfate (ref) excited at the same wavelength), n is the refractive index (1.33 for aqueous dispersions of CQDs and for quinine sulfate (ref) in 0.5 M H_2SO_4), and A is the absorbance at 350 nm or 375 nm as appropriate.

3 RESULTS

3.1 Properties of flax by-products

Table 1 shows the ash and moisture contents, as well as those of lignin, cellulose, and hemicellulose, and the corresponding results of elemental analysis (EA). Flax straw contained 2.44% ashes and 9.13% moisture, similar values to those presented in former studies (Hasan Khan Tushar et al., 2012), while the flax powder contained 7.66% ash and 10.69% moisture. Note the much higher ash content in the flax powder. The lignin, cellulose and hemicellulose contents in the flax powder were 43, 25 and 32%, respectively, and 40, 39 and 21%, respectively, in the flax straw. The latter compositions were also within the ranges found in the literature (Tamaki and Mazza, 2010). The higher ash and hemicellulose content in flax powder will account for the less developed textural properties and lower carbon yield obtained from it, see below. In terms of EA, the main difference is the much higher nitrogen content of flax powder, 1.71%, compared to that of flax fibers, which are more oxygen-rich.

Table 1. Composition of flax powders and fibers.

	Ash (wt.%)	**Moisture (wt.%)**	**Lignin (wt.%)**	**Cellulose (wt.%)**	**Hemicellulose (wt.%)**	**C (wt.%)**	**H (wt.%)**	**N (wt.%)**	**S (wt.%)**	**O* (wt.%)**
Powder	7.66	10.69	43	25	32	48.82	7.20	1.71	0.05	38.33
Fibers	2.44	9.13	40	39	21	48.36	6.38	0.30	0.00	44.18

* Directly determined

Figure 1 shows the morphology of the ashes from the flax powder; they have a very small particle size (Figure 1(a)), while those from the flax fibers (Figure 1(b)) retain the fiber shape. Figure S1 and Figure S2 show the elemental mapping of the major elements. This kind of analysis can never be strictly considered as quantitative, but it gives information about the composition of the ashes. Moreover, the elemental content depends on the area chosen for analysis and sometimes is very different from one point to another, exacerbated by the fact that the surface is not perfectly flat. This suggests that the materials are very heterogeneous on a small scale. However, it seems clear that potassium and silicon contents are higher in flax fiber-derived ashes.

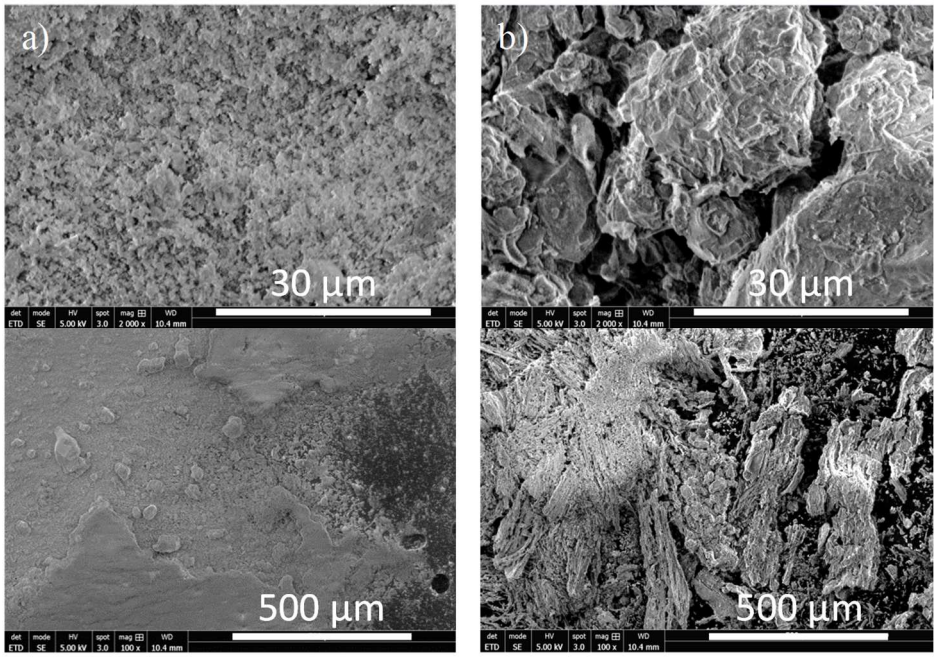

Figure 1. SEM photographs of the ashes from: (a) flax powder; and (b) flax fibers.

Finally, the tapped density was 0.11 g/mL (110 kg/m^3) for flax powder and 0.05 g/mL (50 kg/m^3) for flax fiber. This suggests that the transportation cost would be doubled when shipping the same mass of fiber compared to powder flax.

3.2 Properties of hydrochars

The flax powder was subjected to HTC at severities corresponding to the following conditions of temperature and time: T = 130, 140, 150, 160 or 180 °C, and t = 1, 2, 4, 6, 12 or 24 h. Figure 2(a) shows the hydrochar yields obtained when flax powder was subjected to HTC at different temperatures as a function of severity. The general trend was a decrease in hydrochar yield with increasing temperature and time due to depolymerization reactions occurring during HTC (Sadaka et al., 2014). Figure 2(a) shows that the hydrochar yield decreased from 98.1% at severity 2.66 to 65.0% at severity 5.51.

Figure 2(b) shows selected hydrochar yields from flax powder as well as from flax fibers. In the case of flax fibers, HTC pressure and temperature conditions corresponding to selected severities across the range studied for flax powder were applied (namely: 2.96, 3.44, 3.85, 4.44, 4.92 and 5.51). The hydrochar yield decreased with increasing severity for both kinds of flax by-products, but the effect was greater for flax powder than for flax fiber, 64.97 and 77.27 %, respectively, at severity 5.51. This might be due to the higher hemicellulose content in the flax powder. According to (Peterson et al., 2008), hemicellulose is indeed easily dissolved in water at temperatures above 180 °C and the auto-generated pressure in the present study should also promote the dissolution and hydrolysis of hemicellulose. Mok and Antal Jr (1993) indeed found that it is possible to extract an average of 95% of hemicellulose as monomeric sugars by working at 200-230 °C and in only a few minutes. Moreover, Reza (2011) reported that most of the hemicellulose is extracted, and likely hydrolyzed to monosaccharides at 200 °C in 5 min.

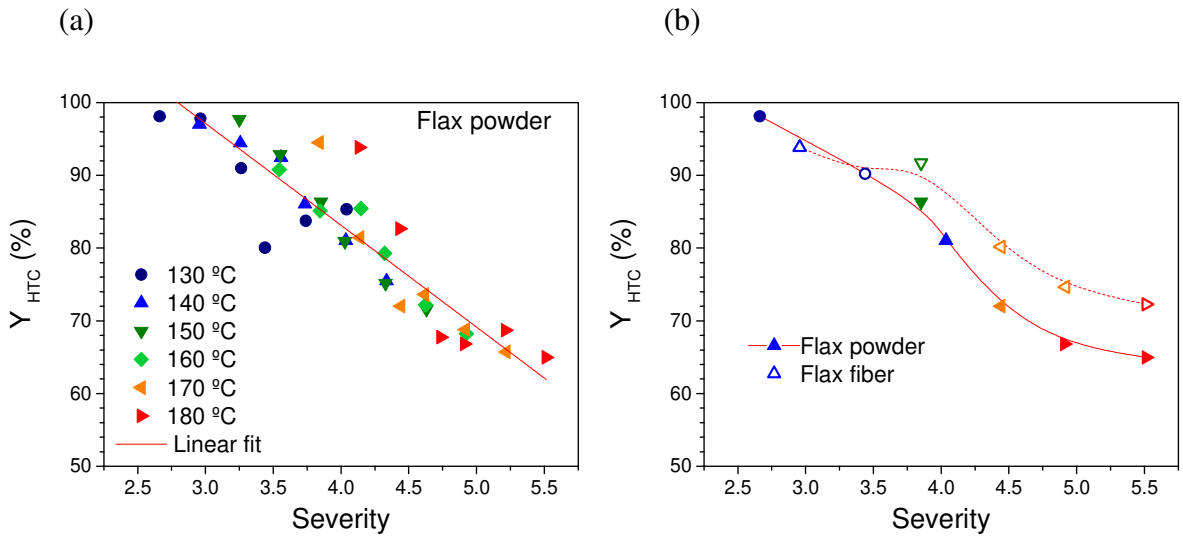

Figure 2. Effect of HTC severity: (a) on the hydrochar yield from flax powder for different operating temperatures; and (b) comparison of hydrochar yields as a function of severity for the two flax precursors.

Figure 3(a) shows the inverse relationship between the O/C atomic ratio and the severity factor. The hydrolysis of cellulose and hemicellulose indeed produces a loss of oxygen and hydrogen, and the corresponding carbon enrichment of the hydrochars (Parshetti et al., 2013).

Figure 3(b) shows the van Krevelen diagram for the hydrochars prepared in this study. The H/C and O/C atomic ratios of the directly pyrolyzed flax powder (*i.e.*, without preliminary HTC) are given as reference (solid black diamond in Figure 3(b)), and are equal to 1.77 and 0.59, respectively. Dehydration (H_2O loss) and decarboxylation (CO_2 loss) reactions during HTC produced some changes in the elemental composition of flax powder-derived hydrochars (Wiedner et al., 2013). Besides, according to the trend observed in the van Krevelen diagram, a dehydration pathway is observed as the HTC severity increases (Xiao et al., 2012). At a low severity of 2.66 (130 °C, 1 h), the composition of the hydrochar (H/C = 1.75; O/C = 0.58) was similar to that of pristine flax powder. At the highest severity, 5.51, a significant change in the elemental composition of the hydrochar was observed (H/C = 1.58; O/C = 0.32). Despite the

range of O/C obtained after HTC, the H/C ratio is higher than those reported for HTC of lignocellulosic biomass (Xiao et al., 2012).

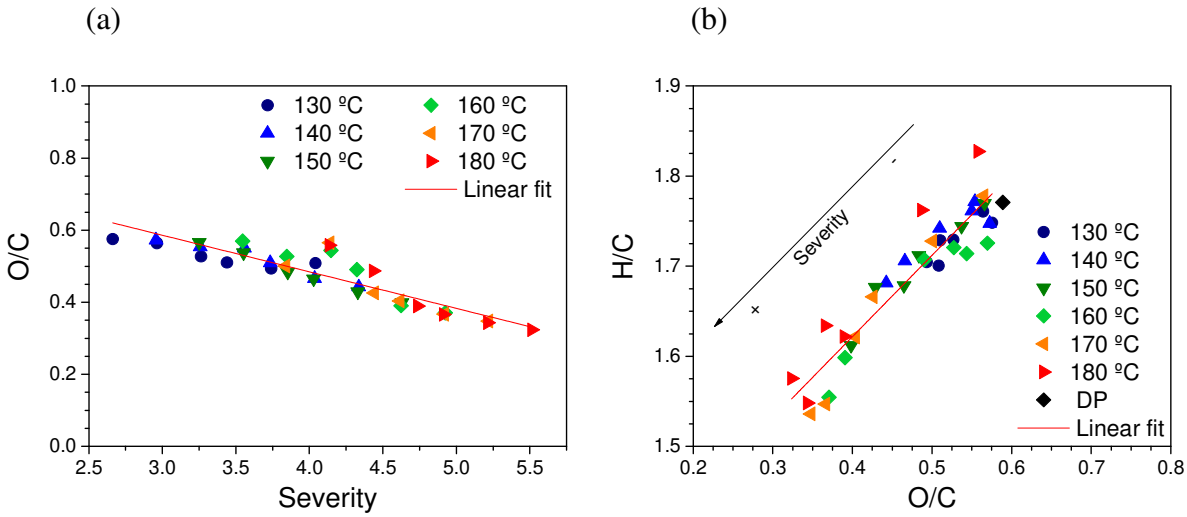

Figure 3. Effect of HTC severity of flax powder on: (a) the atomic O/C ratio; and (b) the Van Krevelen diagram of all materials. DP means directly pyrolyzed at 900 °C, *i.e.*, without HTC step.

The higher heating value (HHV) of the raw flax powder and flax fibers was 21.63 and 19.74 MJ/kg, respectively. Figure 4 shows, for materials submitted to HTC, that the HHV increased linearly with the severity of the process for the two flax-derived hydrochars. It ranged from 22.08 to 27.06 MJ/kg for the hydrochars derived from flax powder, and from 19.80 to 23.18 MJ/kg for those derived from flax fibers. As seen in Figure 4, the measured HHV values for flax powder-derived hydrochars represent the upper limit of those reported in the literature for different biomasses subjected to HTC (Table S1) within the same severity range. Likewise, those of flax fiber-derived hydrochars are in the range of previously reported values. For instance, lipid-extracted algae subjected to HTC at a severity of 5.60 had an HHV of 23.58 MJ/kg (Lee et al., 2018), lower than that of flax powder and only slightly higher than that of flax straw.

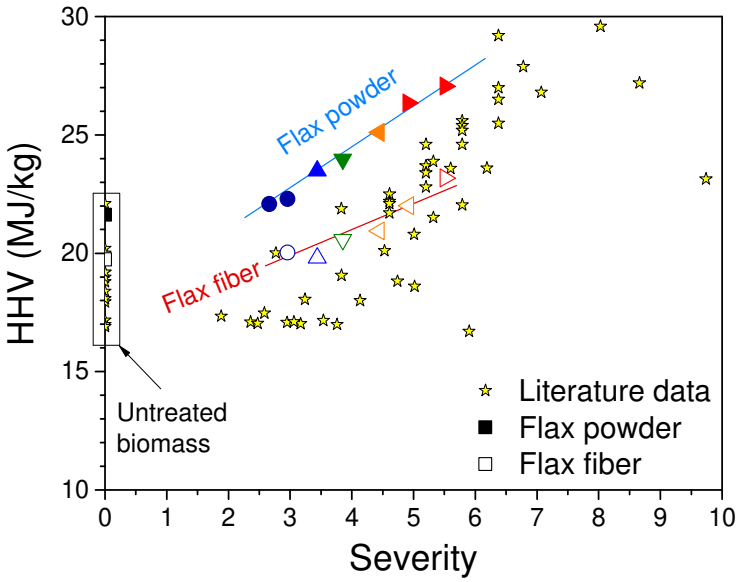

Figure 4. Variation of HHV with severity for raw flax by-products ("untreated biomass") and for the two flax-derived hydrochars. The HHV values of the biomasses and hydrochars obtained by HTC (Table S1) are also included.

The ash contents of the raw materials by TGA were also determined and compared to those obtained by application of ASTM standards, already shown in Table 1. The ash contents of the flax powder and fibers were 6.75 and 1.75 wt.% on a dry basis; these values are somewhat lower than those obtained in the muffle furnace, 7.66 and 2.44 wt.%, respectively, because the ash contents measured in the latter apparatus were obtained at 600 °C, instead of 900 °C with TGA. After the hydrothermal treatment, the ash contents were 5.82 and 0.72 wt.%, respectively. Such a decrease in ash content after HTC can be explained by the partial dissolution of minerals in hot water. Figure S3 shows that the ash contents of flax straw-derived hydrochars decreased from 1.07 to 0.36 wt.% by increasing the severity from 2.96 to 5.51, respectively. No clear trend was observed with flax powder-derived hydrochars when increasing the severity, but the ash content decreased and was 5.82 wt.% on average.

3.3 Properties of the liquid fraction

Selected liquid fractions from the HTC of flax powder were analyzed by GC/MS. Table 2 shows the most important compounds and their concentrations. These organic molecules were 2(*5H*)-furanone, 3-methyl-2(*5H*)-furanone, furfuryl alcohol, 2-acetylfuran, 5-methylfurfural, 5-(hydroxymethyl)furfural and furfural. Figure S4 shows the GC/MS spectrum of the liquid leading to the highest concentration of furfural and 5-methylfurfural, *i.e.*, that obtained at 180 °C and 6 h (severity = 5.51). The substances found in highest concentration were 5-(hydroxymethyl)furfural (5-HMF) and furfural (FU): 0.22 and 0.06 g/L, respectively. Considering the evolution of 5-HMF and FU concentrations with severity, these were maximal at severity 4.91 in both cases. FU is the result of the degradation of hemicelluloses and is classified as one of the main value-added chemicals (Anthonia and Philip, 2015) as it can be used as a selective solvent in the refining of lubricating oils, as a gasoline additive, or as a decolorizing agent. 5-HMF is also a versatile and multifunctional product that can be used as an intermediate in polymer synthesis (Yang et al., 2011). For instance, 5-HMF is used in the production of bioplastics, which are potential substitutes to petroleum-derived plastics commonly used in beverage bottles.

Table 2. Molecules found in the liquids after HTC, and their concentration (g/L)[a] as a function of severity.

Severity	**3.26**	**3.85**	**4.04**	**4.44**	**4.91**	**5.51**
2(*5H*)-Furanone	-	-	-	0.0016	-	0.0015
5-(Hydroxymethyl)Furfural	-	-	0.0123	0.0483	0.2245	0.0255
3-Methyl-2(*5H*)-furanone	-	-	-	-	0.0051	0.0099
Furfuryl alcohol	-	0.0079	0.0234	0.0084	-	-
Furfural	-	-	-	0.0345	0.0558	0.0003
2-Acetylfuran	-	-	-	-	-	0.0036
5-Methylfurfural	-	-	-	0.0218	0.0279	0.0059

[a] = concentration considering the extracted liquid and the water used in the HTC.

3.4 Physicochemical and photoluminescence properties of CQDs

The UV-Vis absorption spectra of CQDs obtained from flax fibers and powder under different HTC severities are shown in Figure 5(a) and Figure 5(b), respectively. Two absorption signals can be distinguished in both series of samples: one with a maximum in the range of 260-290 nm (yellow rectangle) and a second in the range of 295-330 nm (green rectangle). The first absorption peak is the most intense and can be attributed to $\pi \rightarrow \pi^*$ transitions in the aromatic sp^2 carbon network (Li et al., 2011; Tang et al., 2012). The second peak corresponds to the $n \rightarrow \pi^*$ transitions in C=O or C-OH functions (Eda et al., 2010; Zhang et al., 2015). According to these contributions, the existence of both carbon conjugated structure and oxygenated functional groups in CQDs is confirmed. Additionally, the differences between the two sets of samples and between the severities are noticeable. In general, an absorption spectrum with a high contribution from aromatic carbon will in turn have a low contribution from oxygenated groups. The powder-derived CQDs presented a lower contribution from the former and a higher contribution from the latter. This series had a more defective carbon structure due to smaller particle size (more contribution from edges) and more oxygenated groups than the series of fiber-derived CQDs. In result of increasing severity, an increase in the contribution of aromatic carbon (or a decrease in the contribution due to oxygen) is observed for both series. It has indeed been claimed that hydrothermal reduction produces a partial restoration of the aromatic carbon network, going to a greater extent with increasing temperature (Zhou et al., 2009).

The aqueous dispersions of CQDs derived from flax powder and fibers were subjected to various PL excitations to collect the corresponding emission spectra. Figure 5(c) and Figure 5(d) show the PL emission spectra of CQDs obtained from each material by HTC at the highest severity (5.5: 180 °C and 24 h). Lower severities resulted in lower maximum PL emissions. In both cases, the maximum emission wavelength was dependent on the excitation and it redshifted as the excitation wavelength increased. This emission-excitation dependence is due

to the polydispersity of particle sizes and the optical selection of different surface states near the Fermi level of the CQDs when varying the excitation wavelength (Dong et al., 2012; Sun et al., 2006). As an example, Figure 5(e) shows TEM images of the CQDs obtained in this study. The particles are in the range of 5-40 nm and exhibit a spherical-ellipsoidal morphology.

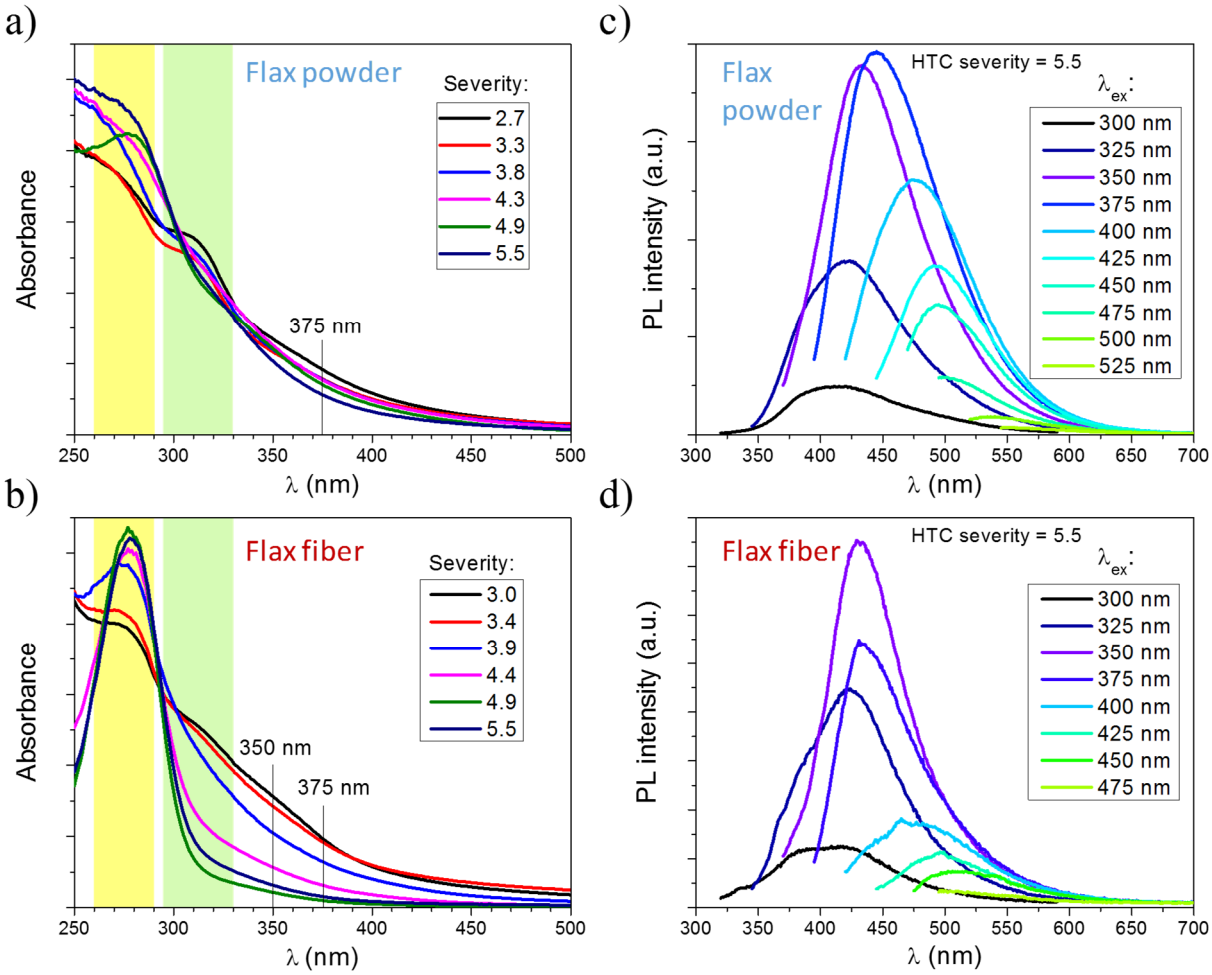

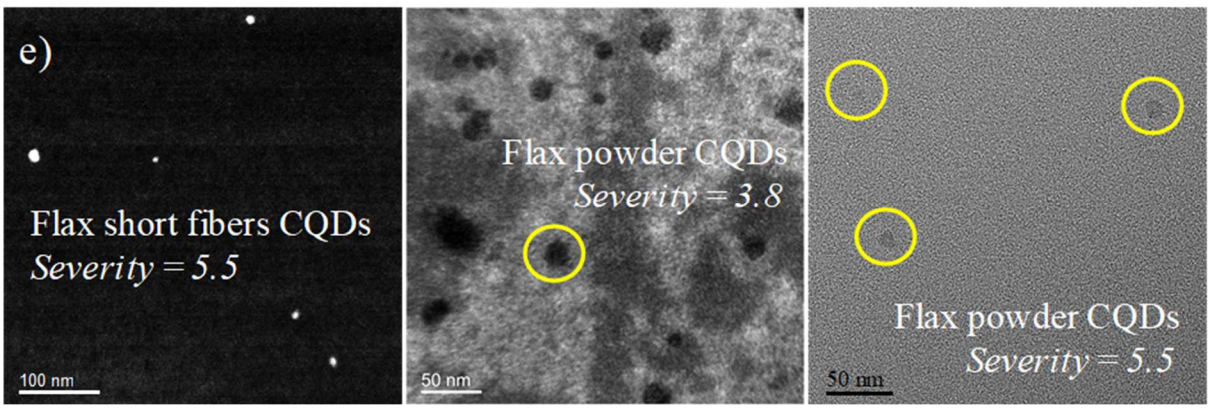

Figure 5. UV-vis absorption of CQDs obtained by HTC at different severities (in the range 2.7-5.5) from: (a) flax powder; and (b) flax short fibers. PL emission spectra of CQDs obtained at the highest severity (5.5) and derived from: (c) flax powder; and (d) flax fiber, using excitation wavelengths ranging from 300 to 520 nm. (e) TEM images of CQDs.

Photographs of aqueous dispersions of CQDs under room light and under UV light illumination are given in Figures 6(a) and 6(b). Strong blue emission can be observed under UV irradiation. The maximum PL emissions for flax fibers- and powder-derived CQDs were located at 430 and 445 nm (both in the violet light region), respectively, after excitation at 350 and 375 nm. Regarding the effect of the severity used in the HTC of the two materials, Figure 6(c) shows the position of the maximum PL emissions of the resulting CQD solutions obtained under severities in the range 2.7-5.5. The position of the maximum emission of flax fibers- and powder-derived CQDs (after excitation at 350 and 375 nm, respectively) shifted to lower wavelengths, from blue (> 450 nm) to violet light (450-400 nm) as the HTC severity increased. It has been demonstrated that PL and emission position depend on the size of sp^2 carbon clusters, which are delimited by oxidation or defects in graphene-like materials (Eda et al., 2010; Loh et al., 2010).

The maximum PL QYs for the two series of CQDs solutions are shown in Figure 6(d). Since the excitations (350 and 375 nm) used to obtain the maximum PL are in the range of quinine sulfate (280-380 nm (Brouwer, 2011)), the latter was used as the reference standard for the determination of PL QY. The PL QY of CQDs increases for both series with the severity of HTC. Increases in temperature or time have been reported to improve PL QY in addition to increasing the weight yield of CQDs (Su et al., 2019). For low severity, PL QY was modest in both series of sample and was around 0.3-0.5 %. The CQDs derived from flax fiber and powder

obtained at the highest HTC severity exhibited PL QYs of 1.1 and 4.7 %, respectively, after excitation at 350 and 375 nm. Comparing these values with those reported in the literature, CQDs obtained by biomass HTC exhibited a wide range of PL QYs depending on the starting material and the severity process. For severities between 4.4 and 5.5, and without the addition of dopants, PL QYs of about 2.8-6.2% are reported for CQDs derived from lignocellulosic materials such as peanut shell, cotton stalk, rice husk, pine wood, soy meal or cellulose (Liu et al., 2020; Thongsai et al., 2019, p.; Zhao et al., 2020). It should also be noted that these PL QYs were measured for extensively purified CQDs, for example by dialysis, which was not performed on the GQDs described in this work. Finally, as observed in Figures 6(e) and 6(f), the flax-derived CQDs showed good photostability under continuous UV irradiation (Hg-Xe lamp, light fluence of 50 mW/cm^2) and a decrease of only 18% of the PL intensity was observed after illumination.

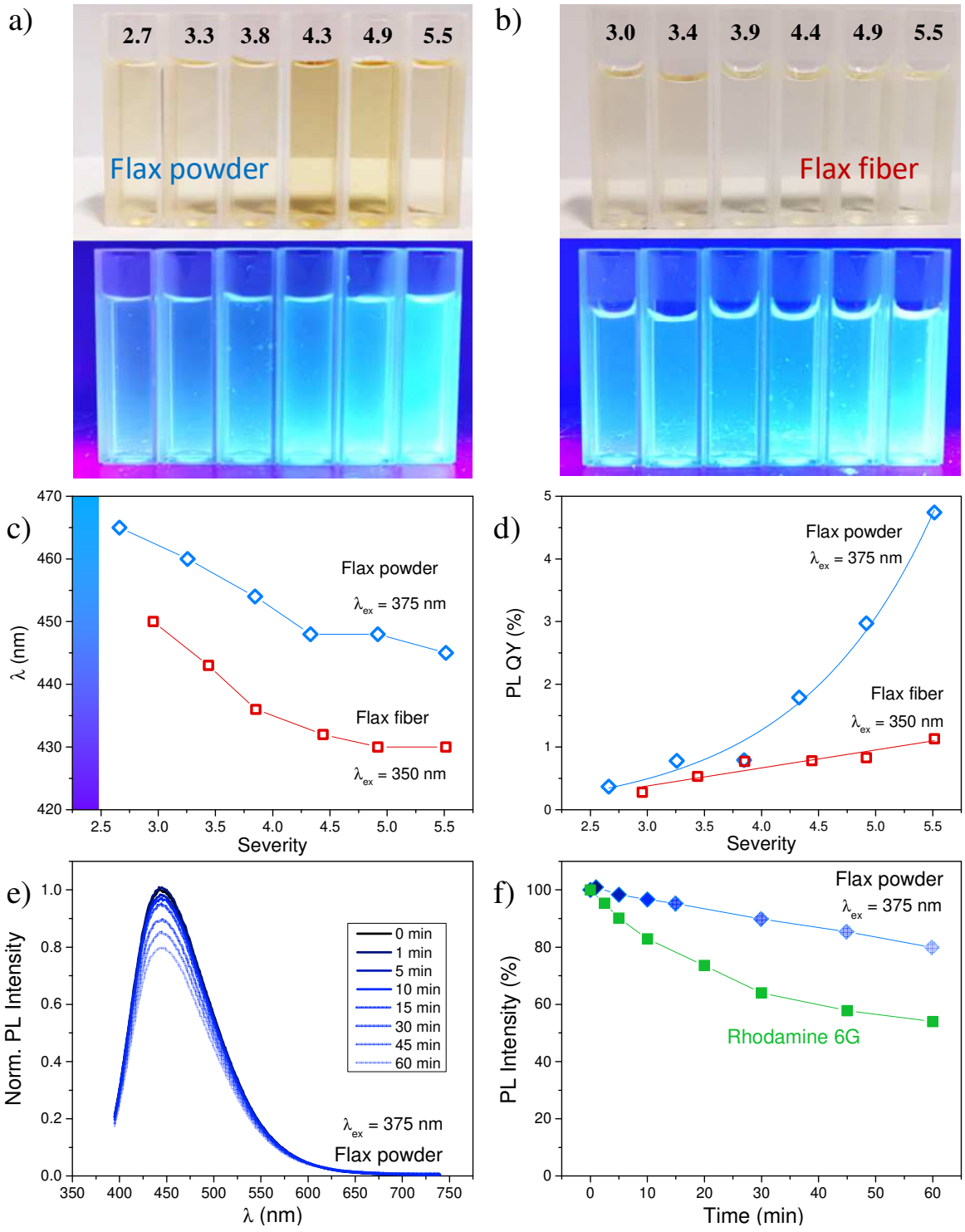

Figure 6. Photographs of aqueous dispersions of CQDs derived from: (a) flax powder; and (b) flax fibres, under (top) room and (bottom) UV lights. (c) Maximum PL positions and (d) PL QYs of the CQD series as a function of HTC severity. (e) and (f) time evolution and photostability of flax powder CQDs (λ_{ex} = 375 nm, HTC severity = 5.5, Hg/Xe lamp; intensity = 50 mW/cm^2).

3.5 Properties of carbonized hydrochars

Selected hydrochar samples were subjected to carbonization; the choice was made based on the severity factor, in order to have a wide range of severities from the lowest to the highest. Figure 7(a) shows that the carbonization yield was always higher for fiber-derived hydrochars than for powder-derived hydrochars. Flax powder directly subjected to carbonization had a carbon yield of 15.1%, whereas after HTC, carbon yields ranged from 16.9 to 24.1%. The increase in carbon yield after HTC is due to dehydration reactions, stabilizing the polyaromatic structure, and to the partial elimination of hemicellulose during HTC (Libra et al., 2011). Flax fiber directly subjected to carbonization had a carbon yield of 25.3%. Flax fiber-derived hydrochars subjected to carbonization yielded higher amounts of carbonaceous materials: the carbon yield ranged from 19.6 to 27.5 %. The lower carbon yield found for the powder-derived materials might be due to their higher ash content, which promotes gasification reactions during carbonization.

Figure 7(b) shows the total yield, considering both the hydrochar yield and the subsequent carbonization yield. Not surprisingly, the total yield was higher for flax fiber; it ranged from 15.7 to 25.3 % versus 12.0 to 17.5% for flax powder. Moreover, the flax fiber-derived carbons were expected to have a lower ash content.

(a) (b)

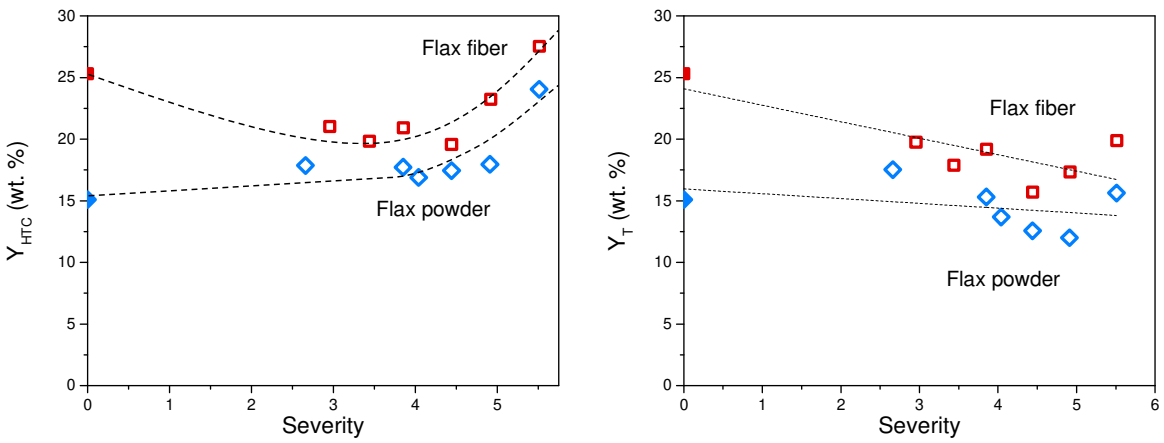

Figure 7. Effect of the severity on: (a) carbonization yield; and (b) total yield of flax powder- and fiber-derived carbons. The dotted lines are just guides for the eye.

Figure 8(a) shows the nitrogen adsorption-desorption isotherms at -196 °C of two carbons produced at 900 °C, one from a flax powder-derived hydrochar and the second from a flax fiber-derived hydrochar, both prepared at a severity of 4.44. The first difference concerns the lower volume of nitrogen adsorbed by the flax powder-derived carbon at $P/P_0 < 0.01$ (corresponding to microporosity), but also at $P/P_0 = 0.97$ (corresponding to total porosity), compared to that derived from flax fiber. The second difference concerns the shape of the isotherms. That of the flax powder-derived carbon presents a sharp slope at $P/P_0 > 0.01$ and a hysteresis cycle; both facts evidence a broad pore size distribution, and the hysteresis indicates the presence of mesopores (pore diameter between 2 and 50 nm). The nitrogen isotherm of the flax fiber-derived carbon is Type Ib according to the IUPAC classification (Thommes et al., 2015), typical of essentially microporous materials with an important fraction of micropores between 0.7 and 2 nm in width. Figure 8(b) shows that the highest pore development of flax fiber-derived carbons compared to those derived from flax powder also involved the narrowest pores (pore diameter < 1.2 nm).

Figure 8(c) shows the pore size distributions (PSDs) while Figure 8(d) shows the cumulated pore volumes, both calculated from the nitrogen and carbon dioxide adsorption data. These plots confirmed the main conclusions extracted from the nitrogen adsorption data, *i.e.*, the essentially microporous character of flax fiber-derived carbons and the micro-mesoporous character of flax powder-derived carbons. Although the microporosity of flax powder-derived carbons is rather narrow, these carbons might be used for pollutant adsorption after activation. The large mesoporous volume would indeed favor the diffusion of pollutants towards the narrowest pores where adsorption takes place. Flax powder-derived carbons could be especially

interesting for adsorbing pollutants from contaminated soils. Moreover, the small particles of flax powder-derived carbons would favor their dispersion in soils.

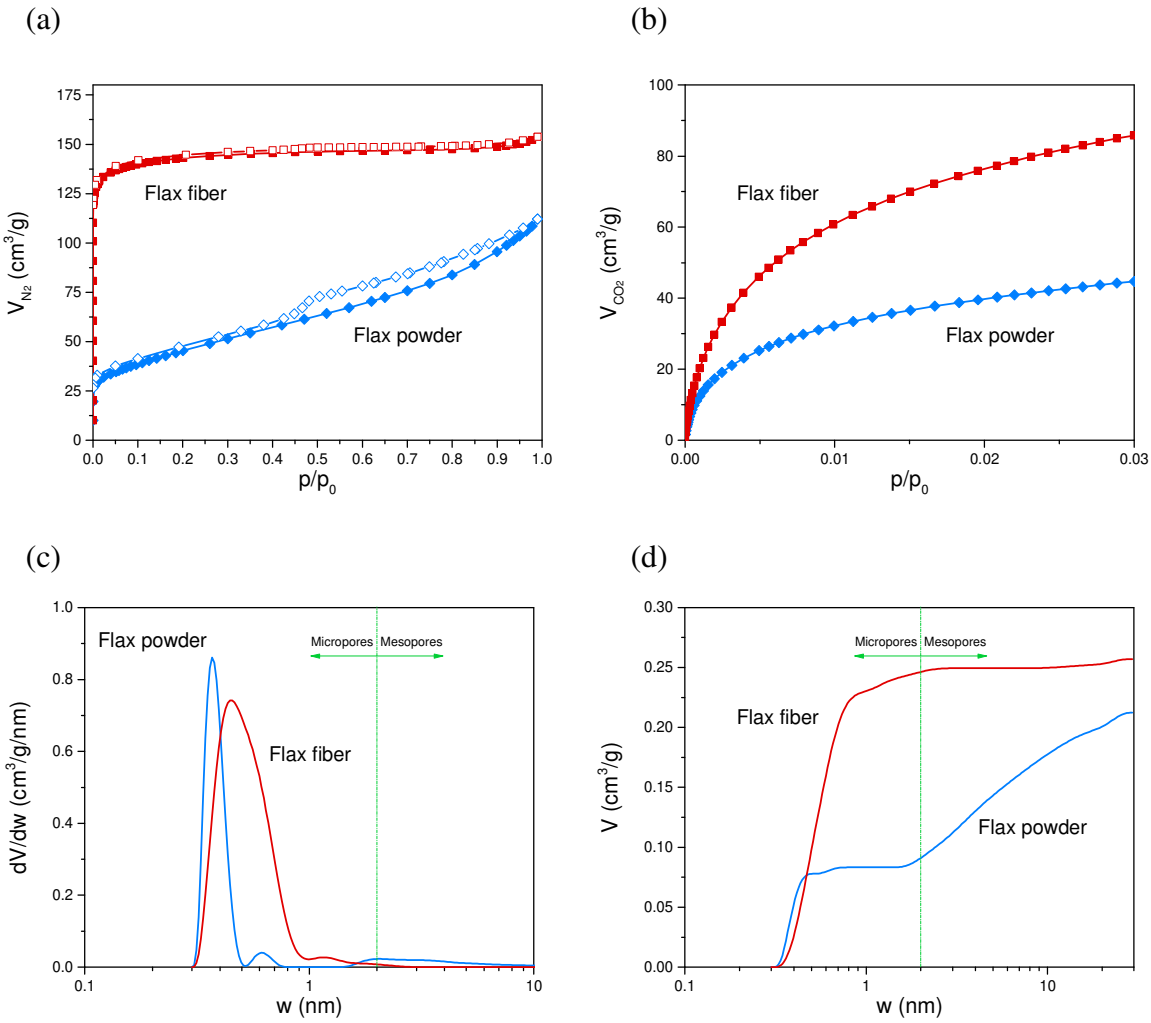

Figure 8. (a) N_2 adsorption-desorption isotherms; and (b) CO_2 adsorption isotherms of carbons produced at 900 °C from flax powder- and fiber-derived hydrochars produced at severity 4.44. (Full symbols: adsorption data, empty symbols: desorption data); (c) pore size distributions; and (d) cumulated pore volumes of the same carbons.

Figure 9 shows the BET area, A_{BET}, of the carbon materials synthesized in this study as a function of severity. Flax fiber-derived carbons had a 2-3 times higher A_{BET} than the flax powder-derived carbons, while the mesoporous volume of the latter was much higher. A

maximum in the mesoporous volume was observed in both carbons for a severity value of 4.92, corresponding to the total degradation of hemicelluloses and to a significant degradation of cellulose, which is totally degraded at a severity equal to 6 (Jeder et al., 2018). The percentage of mesopore volume ranged from 32 to 57% for flax powder-derived carbons while it ranged from 2 to 18% for flax fiber-derived carbons. The higher mesopore volume in the flax powder-derived carbons produced a higher average pore diameter (see also Table S2) than in the flax fiber-derived carbons.

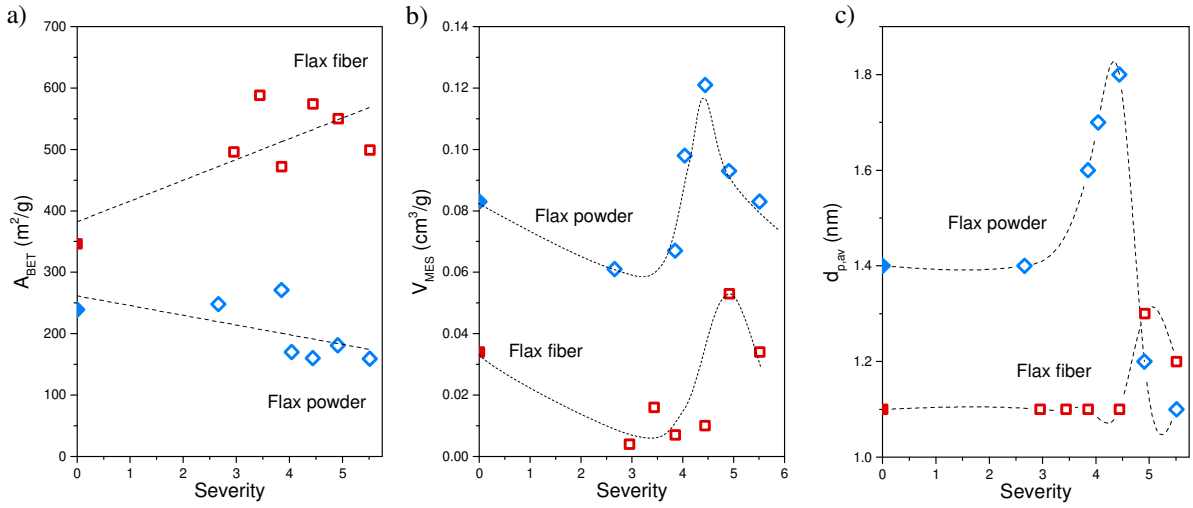

Figure 9. Effect of HTC severity on: (a) A_{BET}, (b) V_{mes}, and (c) $d_{p,av}$ for carbons synthesized at 900 °C from flax powder- and fiber-derived hydrochars. The dotted lines are just guides for the eye.

In summary, Table S2 shows the main textural properties of the carbons synthesized in this study. It can be observed that S_{NLDFT} was always higher than A_{BET}, which is due to the existence of narrow micropores in flax powder- and flax fiber-derived carbons, and to the assumptions of the BET model. In the same way, the micropore volume determined by applying the DR model to the carbon dioxide adsorption data was always higher than that determined by applying the same model to the nitrogen adsorption data. Because carbon dioxide adsorption is carried out

at 0 °C, diffusion of CO_2 molecules is faster than that of N_2 molecules at -196 °C. Higher values of $V_{DR,CO2}$ than those of $V_{DR,N2}$ indicate large volumes of pores narrower than 1.1 nm. As the DR model overestimates the micropore volume, the NLDFT model to calculate the pore size distribution and to determine the micropore volume from both nitrogen and carbon dioxide isotherms has been included here. The total volume estimated by application of the NLDFT model, V_{NLDFT}, was higher than $V_{0.97}$ because the latter only considers the nitrogen adsorption data.

Some of the carbons prepared at 900 °C have a high ultramicropore volume (pore diameter less than 0.7 nm), which could be even higher by using a lower carbonization time. These carbons might be especially interesting for CO_2 capture because they have a developed texture and they are stable under CO_2 capture conditions (García-Díez et al., 2019). Gas physisorption is a completely reversible process and desorption is achieved by lowering the pressure or increasing the temperature (Ramirez-Vidal et al., 2021). Figure 10 shows the CO_2 capture (mmol/g) at 0 °C and 1 bar of carbons prepared by pyrolysis at 900 °C of hydrochars derived from flax powder and fibers, and of some activated and non-activated carbon materials reported in the literature (see also Table S3 in the Supporting Information). For the hydrochar-derived carbons produced from flax powder, the severity of the HTC was a paramount parameter on the resulting CO_2 adsorption capacity. Carbons from hydrochars obtained under severities of 4.9 and above had the highest CO_2 captures. At most, the carbonization of a hydrochar obtained at severity 5.5 from flax powder offered a CO_2 uptake of 4.8 mmol/g, higher than those observed for other non-activated biomass-derived carbons found in the literature (Plaza et al., 2012; Hong et al., 2016; Jeder et al., 2018).

CO_2 adsorption depends on surface area, so that activated carbons (ACs) have generally higher CO_2 capacities than non-activated carbons such as those prepared in this study. However, activation is accompanied by material burn-off and a dramatic decrease in density. Burn-off is

especially high in KOH activation. While it is true that surface areas as high as 2600 m^2/g can be obtained by activation of lignocellulosic precursors, the final yield is close to 5% for biomasses similar to flax (Basta et al., 2008), and close to 10% for those richer in phenolic materials (Fierro et al., 2007). Moreover, the resultant activated carbons present an extremely low density, making them difficult to handle. Burn-off is somewhat lower by physical activation, either with CO_2 or H_2O, but the surface areas are around 1500 m^2/g (Selmi et al., 2018). A second strategy to increase CO_2 adsorption is nitrogen doping in order to increase surface basicity and therefore the interactions between the graphitic domains of the carbon materials and the CO_2 molecules. For this reason, doping with urea (Wu et al., 2016) or sodium amide (Rao et al., 2019; Yang et al., 2019) can be performed. Some materials are naturally rich in nitrogen and can be good candidates as CO_2 adsorbents; this is the case for microalgae (Guo et al., 2017) or flax.

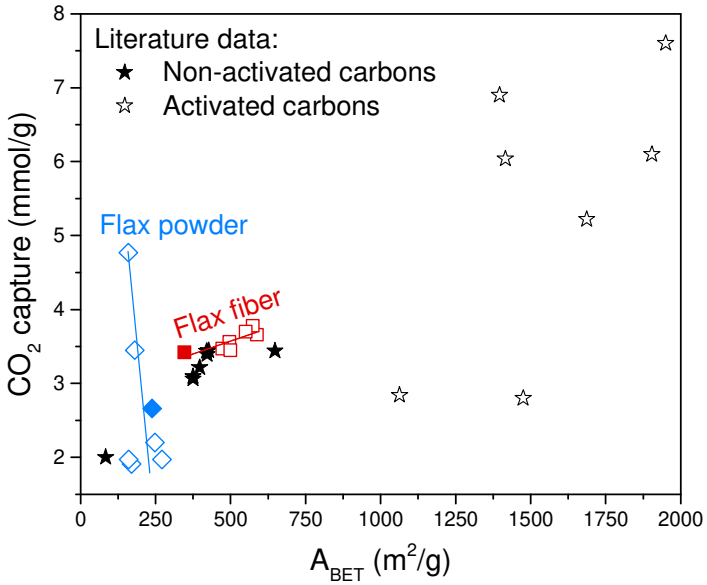

Figure 10. Effect of A_{BET} on CO_2 capture at 0 °C and 1 bar for carbons produced at 900 °C from flax powder- and fiber-derived hydrochars (Full symbols: direct carbonization of the biomass; Lines: guides for the eye). CO_2 adsorption values of biomass-derived, activated and non-activated carbons (see also Table S3) are included.

4 CONCLUSIONS

Flax by-products, namely powder and short fibers, were thoroughly characterized; materials derived from them were prepared and investigated, and applications have been suggested. Their conversion by HTC into liquid fractions, CQDs and hydrochars was also studied. Higher severity, a factor combining time and temperature of HTC, led to carbon-enriched materials, which significantly improved their calorific value. This is especially the case of flax powder-derived hydrochars, whose HHV was among the highest reported in the literature dealing with biomass at similar HTC severity (from 22.1 to 27.1 MJ/kg for severities from 2.7 to 5.5).

The liquid fraction contained organic liquids and dispersed CQDs. The highest yield of 5-hydroxymethylfurfural and furfural, which are considered to be among the most important platform molecules for the future of green chemistry, was obtained at severity of 4.9. On the other hand, CQDs were obtained as rounded nanoparticles of 5-40 nm in diameter, and they exhibited good photoluminescence properties (PL emission and photostability). The CQDs from the two flax by-products: short fibers and powder, showed PL emission at 430 and 445 nm (violet region), respectively, after excitation at 350 and 375 nm. The highest PL quantum yield (4.7%) was measured for the flax powder-derived CQDs at the highest HTC severity (5.5). CQDs have strong potential for bioimaging and healthcare applications.

A broad range of hydrochars derived from both flax by-products were also used to produce carbons by simple pyrolysis at 900 °C. The carbons derived from short flax fibers exhibited the highest surface areas (reaching values of S_{NLDFT} of up to 950 m^2/g), the lowest mesopore volumes (below 18%), the narrowest pore size distributions, and the lowest average pore size (1.1-1.3 nm). All of these carbons can be considered as cheap, yet medium-performance, general-purpose adsorbents. Likewise, the two flax-derived carbons might be used for gas adsorption, particularly CO_2, for which values up to 4.8 mmol/g at 1 bar and 0 °C were obtained without any additional activation step.

Acknowledgements

This study was partly supported by the TALiSMAN project (2019-000214), funded by the European Regional Development Fund (ERDF). The authors thank Christine Gendarme for her technical assistance with the SEM characterization and Philippe Gadonneix for his technical assistance in the laboratory measurements.

REFERENCES

Abbas, A., Mariana, L.T., Phan, A.N., 2018. Biomass-waste derived graphene quantum dots and their applications. Carbon 140, 77–99. https://doi.org/10.1016/j.carbon.2018.08.016

Akin, D.E., 2013. Linen Most Useful: Perspectives on Structure, Chemistry, and Enzymes for Retting Flax [WWW Document]. Int. Sch. Res. Not. https://doi.org/10.5402/2013/186534

Anthonia, E.E., Philip, H.S., 2015. An overview of the applications of furfural and its derivatives. Int. J. Adv. Chem. 3, 42–47. https://doi.org/10.14419/ijac.v3i2.5048

Baley, C., Kervoëlen, A., Le Duigou, A., Goudenhooft, C., Bourmaud, A., 2016. Is the low shear modulus of flax fibres an advantage for polymer reinforcement? Mater. Lett. 185, 534–536. https://doi.org/10.1016/j.matlet.2016.09.067

Basta, A.H., Fierro, V., El-Saied, H., Celzard, A., 2008. 2-Steps KOH activation of rice straw: An efficient method for preparing high-performance activated carbons. Bioresour. Technol. 100, 3941–3947. https://doi.org/10.1016/j.biortech.2009.02.028

Borrero-López, A.M., Masson, E., Celzard, A., Fierro, V., 2020. Modelling the production of solid and liquid products from the hydrothermal carbonisation of two biomasses. Ind. Crops Prod. 151, 112452. https://doi.org/10.1016/j.indcrop.2020.112452

Borrero-López, A.M., Masson, E., Celzard, A., Fierro, V., 2018. Modelling the reactions of cellulose, hemicellulose and lignin submitted to hydrothermal treatment. Ind. Crops Prod. 124, 919–930. https://doi.org/10.1016/j.indcrop.2018.08.045

Braghiroli, F.L., Fierro, V., Izquierdo, M.T., Parmentier, J., Pizzi, A., Celzard, A., 2014. Kinetics of the hydrothermal treatment of tannin for producing carbonaceous microspheres. Bioresour. Technol. 151, 271–277. https://doi.org/10.1016/j.biortech.2013.10.045

Braghiroli, F.L., Fierro, V., Izquierdo, M.T., Parmentier, J., Pizzi, A., Celzard, A., 2012. Nitrogen-doped carbon materials produced from hydrothermally treated tannin. Carbon 50, 5411–5420. https://doi.org/10.1016/j.carbon.2012.07.027

Braghiroli, F.L., Fierro, V., Parmentier, J., Vidal, L., Gadonneix, P., Celzard, A., 2015a. Hydrothermal carbons produced from tannin by modification of the reaction medium: Addition of H+ and Ag+. Ind. Crops Prod. 77, 364–374. https://doi.org/10.1016/j.indcrop.2015.09.010

Braghiroli, F.L., Fierro, V., Szczurek, A., Stein, N., Parmentier, J., Celzard, A., 2015b. Hydrothermally treated aminated tannin as precursor of N-doped carbon gels for supercapacitors. Carbon 90, 63–74. https://doi.org/10.1016/j.carbon.2015.03.038

Braghiroli, F.L., Fierro, V., Szczurek, A., Stein, N., Parmentier, J., Celzard, A., 2015c. Electrochemical performances of hydrothermal tannin-based carbons doped with nitrogen. Ind. Crops Prod. 70, 332–340. https://doi.org/10.1016/j.indcrop.2015.03.046

Brouwer, A.M., 2011. Standards for photoluminescence quantum yield measurements in solution (IUPAC Technical Report). Pure Appl. Chem. 83, 2213–2228. https://doi.org/10.1351/PAC-REP-10-09-31

Brunauer, S., Emmett, P.H., Teller, E., 1938. Adsorption of Gases in Multimolecular Layers. J. Am. Chem. Soc. 60, 309–319. https://doi.org/10.1021/ja01269a023

Catrinck, M.N., Ribeiro, E.S., Monteiro, R.S., Ribas, R.M., Barbosa, M.H.P., Teófilo, R.F., 2017. Direct conversion of glucose to 5-hydroxymethylfurfural using a mixture of niobic acid and niobium phosphate as a solid acid catalyst. Fuel 210, 67–74. https://doi.org/10.1016/j.fuel.2017.08.035

Das, R., Bandyopadhyay, R., Pramanik, P., 2018. Carbon quantum dots from natural resource: A review. Mater. Today Chem. 8, 96–109. https://doi.org/10.1016/j.mtchem.2018.03.003

Dong, Y., Shao, J., Chen, C., Li, H., Wang, R., Chi, Y., Lin, X., Chen, G., 2012. Blue luminescent graphene quantum dots and graphene oxide prepared by tuning the carbonization degree of citric acid. Carbon 50, 4738–4743. https://doi.org/10.1016/j.carbon.2012.06.002

Dou, Y., Zhou, S., Oldani, C., Fang, W., Cao, Q., 2018. 5-Hydroxymethylfurfural production from dehydration of fructose catalyzed by Aquivion@silica solid acid. Fuel 214, 45–54. https://doi.org/10.1016/j.fuel.2017.10.124

Dubinin, M.M., 1989. Fundamentals of the theory of adsorption in micropores of carbon adsorbents: Characteristics of their adsorption properties and microporous structures. Carbon 27, 457–467. https://doi.org/10.1016/0008-6223(89)90078-X

Eda, G., Lin, Y.-Y., Mattevi, C., Yamaguchi, H., Chen, H.-A., Chen, I.-S., Chen, C.-W., Chhowalla, M., 2010. Blue Photoluminescence from Chemically Derived Graphene Oxide. Adv. Mater. 22, 505–509. https://doi.org/10.1002/adma.200901996

Fierro, V., Torné-Fernández, V., Celzard, A., 2007. Methodical study of the chemical activation of Kraft lignin with KOH and NaOH. Microporous Mesoporous Mater. 101, 419–431. https://doi.org/10.1016/j.micromeso.2006.12.004

Funke, A., Ziegler, F., 2010. Hydrothermal carbonization of biomass: A summary and discussion of chemical mechanisms for process engineering. Biofuels Bioprod. Biorefining 4, 160–177. https://doi.org/10.1002/bbb.198

García-Díez, E., Schaefer, S., Sanchez-Sanchez, A., Celzard, A., Fierro, V., Maroto-Valer, M.M., García, S., 2019. Novel Porous Carbons Derived from Coal Tar Rejects: Assessment of the Role of Pore Texture in CO2 Capture under Realistic Postcombustion Operating Temperatures. ACS Appl. Mater. Interfaces 11, 36789–36799. https://doi.org/10.1021/acsami.9b13247

Guo, L.-P., Zhang, Y., Li, W.-C., 2017. Sustainable microalgae for the simultaneous synthesis of carbon quantum dots for cellular imaging and porous carbon for CO2 capture. J. Colloid Interface Sci. 493, 257–264. https://doi.org/10.1016/j.jcis.2017.01.003

Harry, I., Ibrahim, H., Thring, R., Idem, R., 2014. Catalytic subcritical water liquefaction of flax straw for high yield of furfural. Biomass Bioenergy 71, 381–393. https://doi.org/10.1016/j.biombioe.2014.09.017

Hasan Khan Tushar, M.S., Mahinpey, N., Khan, A., Ibrahim, H., Kumar, P., Idem, R., 2012. Production, characterization and reactivity studies of chars produced by the isothermal pyrolysis of flax straw. Biomass Bioenergy 37, 97–105. https://doi.org/10.1016/j.biombioe.2011.12.027

Hong, S.-M., Jang, E., Dysart, A.D., Pol, V.G., Lee, K.B., 2016. CO2 Capture in the Sustainable Wheat-Derived Activated Microporous Carbon Compartments. Sci. Rep. 6, 34590. https://doi.org/10.1038/srep34590

Jagiello, J., Ania, C., Parra, J.B., Cook, C., 2015. Dual gas analysis of microporous carbons using 2D-NLDFT heterogeneous surface model and combined adsorption data of N2 and CO2. Carbon 91, 330–337. https://doi.org/10.1016/j.carbon.2015.05.004

Jeder, A., Sanchez-Sanchez, A., Gadonneix, P., Masson, E., Ouederni, A., Celzard, A., Fierro, V., 2018. The severity factor as a useful tool for producing hydrochars and derived carbon materials. Environ. Sci. Pollut. Res. 25, 1497–1507. https://doi.org/10.1007/s11356-017-0366-7

Kang, S., Li, X., Fan, J., Chang, J., 2012. Solid fuel production by hydrothermal carbonization of black liquor. Bioresour. Technol. 110, 715–718. https://doi.org/10.1016/j.biortech.2012.01.093

Lee, J., Lee, K., Sohn, D., Kim, Y.M., Park, K.Y., 2018. Hydrothermal carbonization of lipid extracted algae for hydrochar production and feasibility of using hydrochar as a solid fuel. Energy 153, 913–920. https://doi.org/10.1016/j.energy.2018.04.112

Li, H., He, X., Liu, Y., Huang, H., Lian, S., Lee, S.-T., Kang, Z., 2011. One-step ultrasonic synthesis of water-soluble carbon nanoparticles with excellent photoluminescent properties. Carbon 49, 605–609. https://doi.org/10.1016/j.carbon.2010.10.004

Li, L., Hale, M., Olsen, P., Berge, N.D., 2014. Using liquid waste streams as the moisture source during the hydrothermal carbonization of municipal solid wastes. Waste Manag. 34, 2185–2195. https://doi.org/10.1016/j.wasman.2014.06.024

Libra, J.A., Ro, K.S., Kammann, C., Funke, A., Berge, N.D., Neubauer, Y., Titirici, M.-M., Fühner, C., Bens, O., Kern, J., Emmerich, K.-H., 2011. Hydrothermal carbonization of biomass residuals: a comparative review of the chemistry, processes and applications of wet and dry pyrolysis. Biofuels 2, 71–106. https://doi.org/10.4155/bfs.10.81

Liu, Y., Zhu, C., Gao, Y., Yang, L., Xu, J., Zhang, X., Lu, C., Wang, Y., Zhu, Y., 2020. Biomass-derived nitrogen self-doped carbon dots via a simple one-pot method: Physicochemical, structural, and luminescence properties. Appl. Surf. Sci. 510, 145437. https://doi.org/10.1016/j.apsusc.2020.145437

Loh, K.P., Bao, Q., Eda, G., Chhowalla, M., 2010. Graphene oxide as a chemically tunable platform for optical applications. Nat. Chem. 2, 1015–1024. https://doi.org/10.1038/nchem.907

Lv, G., Deng, L., Lu, B., Li, J., Hou, X., Yang, Y., 2017. Efficient dehydration of fructose into 5-hydroxymethylfurfural in aqueous medium over silica-included heteropolyacids. J. Clean. Prod. 142, 2244–2251. https://doi.org/10.1016/j.jclepro.2016.11.053

Mok, W.S., Antal Jr, M.J., 1993. Biomass fractionation by hot compressed liquid water, in: Advances in Thermochemical Biomass Conversion. Springer, pp. 1572–1582.

Overend, R.P., Chornet, E., Gascoigne, J.A., 1987. Fractionation of Lignocellulosics by Steam-Aqueous Pretreatments [and Discussion]. Philos. Trans. R. Soc. Lond. Math. Phys. Eng. Sci. 321, 523–536. https://doi.org/10.1098/rsta.1987.0029

Parshetti, G.K., Kent Hoekman, S., Balasubramanian, R., 2013. Chemical, structural and combustion characteristics of carbonaceous products obtained by hydrothermal carbonization of palm empty fruit bunches. Bioresour. Technol. 135, 683–689. https://doi.org/10.1016/j.biortech.2012.09.042

Peterson, A.A., Vogel, F., Lachance, R.P., Fröling, M., Michael J. Antal, J., Tester, J.W., 2008. Thermochemical biofuel production in hydrothermal media: A review of sub- and supercritical water technologies. Energy Environ. Sci. 1, 32–65. https://doi.org/10.1039/B810100K

Plaza, M.G., González, A.S., Pevida, C., Pis, J.J., Rubiera, F., 2012. Valorisation of spent coffee grounds as CO2 adsorbents for postcombustion capture applications. Appl. Energy 99, 272–279. https://doi.org/10.1016/j.apenergy.2012.05.028

Ramirez-Vidal, P., Canevesi, R.L.S., Sdanghi, G., Schaefer, S., Maranzana, G., Celzard, A., Fierro, V., 2021. A Step Forward in Understanding the Hydrogen Adsorption and Compression on Activated Carbons. ACS Appl. Mater. Interfaces 13, 12562–12574. https://doi.org/10.1021/acsami.0c22192

Rao, L., Liu, S., Wang, L., Ma, C., Wu, J., An, L., Hu, X., 2019. N-doped porous carbons from low-temperature and single-step sodium amide activation of carbonized water chestnut shell with excellent CO2 capture performance. Chem. Eng. J. 359, 428–435. https://doi.org/10.1016/j.cej.2018.11.065

Reza, M.T., 2011. Hydrothermal carbonization of lignocellulosic biomass. University of Nevada, Reno.

Román, S., Valente Nabais, J.M., Ledesma, B., González, J.F., Laginhas, C., Titirici, M.M., 2013. Production of low-cost adsorbents with tunable surface chemistry by conjunction of hydrothermal carbonization and activation processes. Microporous Mesoporous Mater. 165, 127–133. https://doi.org/10.1016/j.micromeso.2012.08.006

Sadaka, S., Sharara, M.A., Ashworth, A., Keyser, P., Allen, F., Wright, A., 2014. Characterization of Biochar from Switchgrass Carbonization. Energies 7, 548–567. https://doi.org/10.3390/en7020548

Schaefer, S., Fierro, V., Izquierdo, M.T., Celzard, A., 2016. Assessment of hydrogen storage in activated carbons produced from hydrothermally treated organic materials. Int. J. Hydrog. Energy 41, 12146–12156. https://doi.org/10.1016/j.ijhydene.2016.05.086

Selmi, T., Sanchez-Sanchez, A., Gadonneix, P., Jagiello, J., Seffen, M., Sammouda, H., Celzard, A., Fierro, V., 2018. Tetracycline removal with activated carbons produced by hydrothermal carbonisation of Agave americana fibres and mimosa tannin. Ind. Crops Prod. 115, 146–157. https://doi.org/10.1016/j.indcrop.2018.02.005

Steinbach, D., Kruse, A., Sauer, J., 2017. Pretreatment technologies of lignocellulosic biomass in water in view of furfural and 5-hydroxymethylfurfural production- A review. Biomass Convers. Biorefinery 7, 247–274. https://doi.org/10.1007/s13399-017-0243-0

Steinbeiss, S., Gleixner, G., Antonietti, M., 2009. Effect of biochar amendment on soil carbon balance and soil microbial activity. Soil Biol. Biochem. 41, 1301–1310. https://doi.org/10.1016/j.soilbio.2009.03.016

Su, H., Bi, Z., Ni, Y., Yan, L., 2019. One-pot degradation of cellulose into carbon dots and organic acids in its homogeneous aqueous solution. Green Energy Environ. 4, 391–399. https://doi.org/10.1016/j.gee.2019.01.009

Sun, Y.-P., Zhou, B., Lin, Y., Wang, W., Fernando, K.A.S., Pathak, P., Meziani, M.J., Harruff, B.A., Wang, X., Wang, H., Luo, P.G., Yang, H., Kose, M.E., Chen, B., Veca, L.M., Xie, S.-Y., 2006. Quantum-Sized Carbon Dots for Bright and Colorful Photoluminescence. J. Am. Chem. Soc. 128, 7756–7757. https://doi.org/10.1021/ja062677d

Tamaki, Y., Mazza, G., 2010. Measurement of structural carbohydrates, lignins, and micro-components of straw and shives: Effects of extractives, particle size and crop species. Ind. Crops Prod. 31, 534–541. https://doi.org/10.1016/j.indcrop.2010.02.004

Tang, L., Ji, R., Cao, X., Lin, J., Jiang, H., Li, X., Teng, K.S., Luk, C.M., Zeng, S., Hao, J., Lau, S.P., 2012. Deep Ultraviolet Photoluminescence of Water-Soluble Self-Passivated Graphene Quantum Dots. ACS Nano 6, 5102–5110. https://doi.org/10.1021/nn300760g

Thommes, M., Kaneko, K., Neimark, A.V., Olivier, J.P., Rodriguez-Reinoso, F., Rouquerol, J., Sing, K.S.W., 2015. Physisorption of gases, with special reference to the evaluation of surface area and pore size distribution (IUPAC Technical Report). Pure Appl. Chem. 87, 1051–1069. https://doi.org/10.1515/pac-2014-1117

Thongsai, N., Tanawannapong, N., Praneerad, J., Kladsomboon, S., Jaiyong, P., Paoprasert, P., 2019. Real-time detection of alcohol vapors and volatile organic compounds via optical electronic nose using carbon dots prepared from rice husk and density functional theory calculation. Colloids Surf. Physicochem. Eng. Asp. 560, 278–287. https://doi.org/10.1016/j.colsurfa.2018.09.077

Titirici, M.-M., White, R.J., Falco, C., Sevilla, M., 2012. Black perspectives for a green future: hydrothermal carbons for environment protection and energy storage. Energy Environ. Sci. 5, 6796–6822. https://doi.org/10.1039/C2EE21166A

Wei, L., Sevilla, M., Fuertes, A.B., Mokaya, R., Yushin, G., 2011. Hydrothermal Carbonization of Abundant Renewable Natural Organic Chemicals for High-Performance Supercapacitor Electrodes. Adv. Energy Mater. 1, 356–361. https://doi.org/10.1002/aenm.201100019

Wiedner, K., Naisse, C., Rumpel, C., Pozzi, A., Wieczorek, P., Glaser, B., 2013. Chemical modification of biomass residues during hydrothermal carbonization – What makes the difference, temperature or feedstock? Org. Geochem. 54, 91–100. https://doi.org/10.1016/j.orggeochem.2012.10.006

Wu, Q., Li, W., Liu, S., Jin, C., 2016. Hydrothermal synthesis of N-doped spherical carbon from carboxymethylcellulose for CO2 capture. Appl. Surf. Sci. 369, 101–107. https://doi.org/10.1016/j.apsusc.2016.02.022

Xiao, L.-P., Shi, Z.-J., Xu, F., Sun, R.-C., 2012. Hydrothermal carbonization of lignocellulosic biomass. Bioresour. Technol. 118, 619–623. https://doi.org/10.1016/j.biortech.2012.05.060

Yan, L., Chouw, N., Jayaraman, K., 2014. Flax fibre and its composites – A review. Compos. Part B Eng. 56, 296–317. https://doi.org/10.1016/j.compositesb.2013.08.014

Yang, L., Liu, Y., Ruan, R., Wang, Y., Zeng, W., Liu, C., Zhang, J., 2011. Advances in production of 5-hydroxymethylfurfural from starch. Xiandai HuagongModern Chem. Ind. 31, 32–36.
Yang, Z., Zhang, G., Xu, Y., Zhao, P., 2019. One step N-doping and activation of biomass carbon at low temperature through NaNH2: An effective approach to CO2 adsorbents. J. CO2 Util. 33, 320–329. https://doi.org/10.1016/j.jcou.2019.06.021
Yemiş, O., Mazza, G., 2011. Acid-catalyzed conversion of xylose, xylan and straw into furfural by microwave-assisted reaction. Bioresour. Technol. 102, 7371–7378. https://doi.org/10.1016/j.biortech.2011.04.050
Yoshimura, M., Byrappa, K., 2008. Hydrothermal processing of materials: past, present and future. J. Mater. Sci. 43, 2085–2103. https://doi.org/10.1007/s10853-007-1853-x
Zhang, Y., He, Y.H., Cui, P.P., Feng, X.T., Chen, L., Yang, Y.Z., Liu, X.G., 2015. Water-soluble, nitrogen-doped fluorescent carbon dots for highly sensitive and selective detection of Hg2+ in aqueous solution. RSC Adv. 5, 40393–40401. https://doi.org/10.1039/C5RA04653J
Zhao, S., Song, X., Chai, X., Zhao, P., He, H., Liu, Z., 2020. Green production of fluorescent carbon quantum dots based on pine wood and its application in the detection of Fe3+. J. Clean. Prod. 263, 121561. https://doi.org/10.1016/j.jclepro.2020.121561
Zhou, Y., Bao, Q., Tang, L.A.L., Zhong, Y., Loh, K.P., 2009. Hydrothermal Dehydration for the “Green” Reduction of Exfoliated Graphene Oxide to Graphene and Demonstration of Tunable Optical Limiting Properties. Chem. Mater. 21, 2950–2956. https://doi.org/10.1021/cm9006603

Upgrading of flax powder and short fibers into high value-added products

Torres et al.

Graphical Abtract